Journal of Nanobiotechnology

RESEARCH Open Access

# Hyaluronic acid-coated polypeptide nanogel enhances specific distribution and therapy of tacrolimus in rheumatoid arthritis

Yuhuan Li[1†], Xin Wang[2†], Yu Gao[1,2], Ziyi Zhang[1], Te Liu[3,4], Zhuo Zhang[1], Yinan Wang[5], Fei Chang[2*] and Modi Yang[1*]

**Abstract**

Rheumatoid arthritis (RA) involves chronic inflammation, oxidative stress, and complex immune cell interactions, leading to joint destruction. Traditional treatments are often limited by off-target effects and systemic toxicity. This study introduces a novel therapeutic approach using hyaluronic acid (HA)-conjugated, redox-responsive polyamino acid nanogels (HA-NG) to deliver tacrolimus (TAC) specifically to inflamed joints. The nanogels' disulfide bonds enable controlled TAC release in response to high intracellular glutathione (GSH) levels in activated macrophages, prevalent in RA-affected tissues. In vitro results demonstrated that HA-NG/TAC significantly reduced TAC toxicity to normal macrophages and showed high biocompatibility. In vivo, HA-NG/TAC accumulated more in inflamed joints compared to non-targeted NG/TAC, enhancing therapeutic efficacy and minimizing side effects. Therapeutic evaluation in collagen-induced arthritis (CIA) mice revealed HA-NG/TAC substantially reduced paw swelling, arthritis scores, synovial inflammation, and bone erosion while suppressing pro-inflammatory cytokine levels. These findings suggest that HA-NG/TAC represents a promising targeted drug delivery system for RA, offering potential for more effective and safer clinical applications.

**Keywords** Rheumatoid arthritis, Reduction-responsive polypeptide nanogel, Hyaluronic acid, Active targeting, Tacrolimus

## Introduction

Rheumatoid arthritis (RA) is a chronic autoimmune disorder characterized by ongoing synovial inflammation, leading to joint damage and disability. Affecting about 1% of the global population, RA predominantly impacts women and individuals aged 30 to 50. The disease presents with joint pain, swelling, and stiffness, often accompanied by fatigue and fever. The exact cause of RA is not fully understood, but it likely involves genetic, environmental, and hormonal factors [1–3]. The disease's pathophysiology involves immune system dysregulation, resulting in synovial proliferation, infiltration, and damage to cartilage and bone. Key immune cells, including T cells, B cells, and macrophages, release pro-inflammatory cytokines like tumor necrosis factor-alpha (TNF-α)

†Yuhuan Li and Xin Wang contributed equally to this work.

*Correspondence:
Fei Chang
changfei@jlu.edu.cn
Modi Yang
yangmodi@jlu.edu.cn
[1]Department of Orthopedics, China-Japan Union Hospital of Jilin University, Changchun 130033, PR China
[2]Department of Orthopedics, The Second Hospital of Jilin University, Changchun 130041, PR China
[3]Scientific Research Center, China-Japan Union Hospital of Jilin University, Changchun, Jilin, China
[4]Yibin Jilin University Research Institute, Jilin University, Yibin, Sichuan, China
[5]Department of Biobank, Division of Clinical Research, The First Hospital of Jilin University, Changchun, China

and interleukin-6 (IL-6), sustaining inflammation [4]. Chronic inflammation in RA not only damages joint tissues but also increases the risk of cardiovascular diseases, osteoporosis, and other comorbidities. Current treatments mainly involve disease-modifying anti-rheumatic drugs (DMARDs) to regulate immune cells and interrupt cytokine pathways, slowing disease progression. These drugs are divided into conventional synthetic DMARDs (csDMARDs) like methotrexate and biologic DMARDs (bDMARDs) such as TNF inhibitors [5]. For example, Tacrolimus (TAC), a strong immunosuppressive agent, needs high doses for effectiveness in RA, leading to systemic immunosuppression and renal toxicity with long-term use [6–8]. Thus, new strategies are needed to enhance drug delivery to inflamed joints while reducing side effects.

In RA, chronic inflammation in the joints raises reactive oxygen species (ROS) levels, leading to oxidative stress, which worsens tissue damage and sustains the inflammatory cycle [9]. Persistent oxidative stress within the synovium damages cellular components like lipids, proteins, and DNA, further activating immune cells and contributing to RA progression [10, 11]. Glutathione (GSH) is a crucial intracellular antioxidant that helps combat oxidative stress. Initially, GSH levels may rise to counteract the increased oxidative environment, but prolonged oxidative stress can deplete GSH, compromising the cell's ability to mitigate oxidative damage [12, 13]. This change in GSH levels is critical in RA, where chronic inflammation continuously challenges the redox balance within cells [14]. However, this change also presents an opportunity to target activated immune cells, which exhibit high levels of proliferation, differentiation, and short lifespans, resulting in higher intracellular GSH expression compared to resting immune and stromal cells [15, 16].

One promising approach to improve targeted drug delivery is nanoparticle-based systems. These systems encapsulate drugs within nanometer-scale particles, enhancing biocompatibility and prolonging circulation time in the bloodstream [17]. In RA, chronic inflammation increases vascular permeability in affected joints, facilitating nanomedicine accumulation through the enhanced permeability and retention (EPR) effect [18, 19]. Polyamino acids allow for precise control over polymer sequence and structure, linking amino acids and their derivatives through amide bonds, ensuring excellent biocompatibility and biodegradability [20–22]. Incorporating disulfide bonds formed between L-cysteines enhances the nanogel structure's stability. These bonds degrade in the presence of reductive agents like GSH. In the inflammatory environment, drug-loaded polyamino acid nanogels are taken up by activated immune cells. High GSH levels in these cells trigger disulfide bond degradation, releasing the drug specifically within pro-inflammatory cells while sparing healthy tissues. This targeted release mechanism ensures precise nanodrug delivery, enhancing therapeutic efficacy and minimizing side effects.

However, passive targeting alone is insufficient for selectively targeting inflammatory cells, as nanoparticles can also be taken up by normal cells, potentially causing unintended effects [23]. Active targeting mechanisms involve ligands that bind specifically to receptors on target cell surfaces [24]. Hyaluronic acid (HA), a naturally occurring polysaccharide, shows promise as a targeting ligand due to its ability to bind to CD44 receptors highly expressed on epithelial and immune cells in inflamed tissues. HA's biocompatibility and multiple functional groups for conjugation make it an attractive candidate for enhancing nanomedicine specificity [25, 26].

In this study, we developed a novel delivery system, NG/TAC, using 1-hexanamine-poly(L-lysine-co-L-cystine) to regulate TAC release in inflamed joints. To enhance targeting of activated macrophages, HA was conjugated with NG/TAC (HA-NG/TAC) for active targeting. Upon reaching the inflammatory environment, HA-NG/TAC is taken up by activated macrophages, where elevated GSH levels trigger disulfide bond degradation in the nanogel framework. This ensures high TAC concentration specifically in inflamed joints, especially in activated macrophages, maximizing immunosuppression efficacy while minimizing systemic toxicity. The effectiveness of this targeted delivery system was evaluated in vivo using a collagen-induced arthritis (CIA) mouse model. The therapeutic potential of HA-NG/TAC was assessed by examining arthritis severity and pro-inflammatory cytokine levels, providing insights into its capacity to improve RA treatment outcomes.

## Method and material

### Materials

We used the following materials: CCK-8 assay kit (Beyotime, C0037), ELISA kits for IL-1β, IL-6, and TNF-α (Proteintech, KE10003, KE10091, KE10002), Strand cDNA Synthesis Super Mix kit (Yeasen, 11119ES60), qPCR SYBR Green Master Mix (Yeasen, 11203ES08), Tacrolimus (Aladdin, T101160), DAPI (Beyotime, C1006), SF488-Phalloidin (Solarbio, CA1640), and Cy5.5 (TOPSCIENCE, TD0091). Supplementary Tables 1 and 2 provide further details on antibodies and primer sequences.

### Cells and animals

We obtained RAW 264.7, MH7A, and HUVEC cells from the American Type Culture Collection (ATCC). These cells were cultured in Dulbecco's minimum essential medium (DMEM, Gibco) supplemented with 10% fetal bovine serum (FBS, Gibco), 1% penicillin (100 IU/

mL, Corning), and streptomycin (100 μg/mL, Corning). Eight-week-old male DBA/1J mice were purchased from Beijing Vital River Laboratory Animal Technology Co., Ltd. The mice were kept under a 12-hour light/dark cycle at a temperature of 25±2 °C and humidity of 60±10%. The Institutional Animal Care and Use Committee of the Chinese Academy of Sciences approved the animal experiment protocols, which complied with relevant ethical regulations.

#### Preparation and characterization of HA-NG/TAC

A mixture of 1-hexylamine and N-carboxy anhydrides of L-lysine (NCA) at a molar ratio of 1:6 was combined in a flame-dried flask and dissolved in anhydrous DMF. The blend was agitated at 25 °C for 72 h, resulting in ring-opening polymerization (ROP) of L-lysine NCA, facilitated by 1-hexylamine as the macroinitiator. L-lysine and L-cystine were then added at a molar ratio of 10:5, and the mixture was agitated at 25 °C for another 72 h to obtain NG (1-hexamine-poly(L-Lysine-co-L-Cystine)). The nanogel precipitate was washed twice with diethyl ether, dried under vacuum for 72 h at room temperature, dissolved in trifluoroacetic acid (TFA), and mixed with hydrobromic acid/acetic acid (HBr/Hac) (33 wt%). After stirring for 1.5 h at 25 °C, the mixture was dialyzed in a dialysis bag (MWCO 500 Da) for 24 h and freeze-dried. NG/TAC was obtained by mixing 1-hexanamine-poly(L-Lysine-co-L-Cystine) with TAC in DMF and agitating for 24 h. HA-NG/TAC was produced by mixing NG/TAC with HA until the solution became homogeneous and transparent. The morphology of HA-NG/TAC was observed using transmission electron microscopy (TEM). Dynamic laser scattering (DLS) measured the hydrodynamic sizes and zeta potentials of NG/TAC and HA-NG/TAC.

#### In vitro TAC loading and release from HA-NG

We calculated the drug loading content (DLC%) of TAC-loaded HA-NG using the equation:

$$DLC\% = \frac{amount\ of\ TAC\ in\ HA-NG}{amount\ of\ HA-NG/TAC} \times 100\%$$

The release behaviors of HA-NG/TAC were investigated in vitro using PBS with 0.5% (v/v) Tween 80 solution at pH 7.4. Freeze-dried HA-NG/TAC was suspended in 5 mL of PBS with 0 or 10 mM GSH inside a dialysis bag (MWCO 3500 Da). During the release trial, the dialysis bag was submerged in 50 mL of PBS with either 0 or 10 mM GSH and agitated at 70 rpm. At predetermined intervals, 2 mL of the external release medium were extracted and replaced with an equal volume of fresh medium. The released drug amount was measured by high-performance liquid chromatography (HPLC) using standard curves at 311 nm.

#### Actively targeting of HA-NG/TAC in vitro

To establish an inflammatory condition, RAW 264.7 cells were stimulated with lipopolysaccharide (LPS) for 24 h, while untreated macrophages served as the control group. Subsequently, macrophages were incubated with Cy5.5-NP and Cy5.5-labeled HA-NG for 4 h. Cells were fixed with 4% paraformaldehyde for 15 min, treated with SF488-Phalloidin for 15 min, followed by a 5-minute incubation with DAPI, and then analyzed using confocal laser scanning microscopy (CLSM). The fluorescence intensity was measured using ImageJ software. RAW 264.7, MH7A, and HUVEC cells were cultured for 24 h and stimulated with LPS for an additional 24 h. The cells were then incubated with Cy5.5-labeled HA-NG for 4 h, fixed for 15 min, stained with DAPI, and observed by CLSM. Fluorescence intensity was analyzed using ImageJ software.

#### Toxicity of HA-NG/TAC in vitro

RAW264.7 cells were cultured at 37 °C for 24 h. Different concentrations of NG/TAC, HA-NG/TAC, and TAC were administered and incubated for 24 h. Additionally, RAW 264.7, MH7A, and HUVEC cells were cultured for 24 h. HA-NG/TAC was introduced and incubated for 48 h and 72 h, respectively. After adding the CCK-8 reagent and incubating at 37 °C for 2 h, the optical density at 450 nm was measured using a microplate reader.

#### Hemolysis test

Fresh blood was centrifuged, and the serum was removed. The blood cells were dispersed in 4 mL of NaCl solution and centrifuged at 1500 rpm for 10 min. Next, 200 μL of this solution was diluted with NaCl to 10 mL. HA-NG/TAC was added to the blood cells to achieve final concentrations ranging from 0.01 μg/mL to 100 μg/mL through serial dilutions. Additionally, washed blood was dissolved in 1 mL of water as a positive control and in 1 mL of NaCl as a negative control. All solutions were incubated in a 37 °C water bath for 2 h, then centrifuged at 6000 rpm for 10 min. The states were photographed and recorded, and the supernatant was collected into a quartz cuvette. Absorbance at 540 nm was measured using a UV spectrophotometer, and the hemolysis rate was calculated using the formula:

$$Hemolysis = \frac{Abs_{Sample} - Abs_{Negative\ control}}{Abs_{Positive\ control} - Abs_{Negative\ control}} \times 100\%$$

where $Abs_{positive\ control}$ is the absorbance of the positive control group, $Abs_{negative\ control}$ is the absorbance of the

negative control group, and $Abs_{sample}$ is the absorbance of the test sample group.

#### Western blot

CD44 was extracted from RAW 264.7, MH7A, and HUVEC cells using RIPA buffer with 1 μM PMSF. Protein concentrations in the supernatant were measured using a BCA protein assay kit and analyzed by Western blot. After separation by 10% SDS-PAGE, the proteins were transferred onto PVDF membranes. The membranes were blocked with Blocking Buffer for Western Blot at room temperature for 10 min and incubated with primary antibodies for CD44 (Proteintech, 15675-1-AP) at 4 °C overnight. They were then treated with HRP-labeled secondary antibodies at room temperature for 1 h. Finally, the bands were detected using an ECL reagent and visualized with a chemiluminescence imaging system.

### 2.9. Establishment of collagen-induced arthritis mouse model

The CIA mouse model was established according to a previous study using eight-week-old male DBA/1J mice [27]. Bovine type II collagen was emulsified with complete Freund's adjuvant containing 2 mg/mL of *Mycobacterium tuberculosis*. The mixture was subcutaneously administered to DBA/1 mice at the base of the tail. After 21 days from the initial injection, the mice received an additional injection of type II collagen mixed with incomplete Freund's adjuvant near the primary injection site.

#### Specific distribution of HA-NG/TAC in vivo

After reaching an average clinical score of 14, the mice with CIA were injected with Cy5.5-labeled NG and Cy5.5-labeled HA-NG via the tail vein. The in vivo imaging system was used to observe the fluorescence image in vivo at the 0.5th, 3th, 6th, 12th, 24th hour post-injection. Subsequently, the mice were euthanized, and their vital organs, such as the heart, liver, spleen, lungs, kidneys, and joints, were collected and examined using the in vivo imaging system. The inflamed paws were fixed in 4% paraformaldehyde and decalcified using a 20% (w/v) ethylenediaminetetraacetic acid (EDTA) solution, with daily changes for 30 days. Subsequently, the joints were sectioned, stained with AF488-CD86 antibody and DAPI, and examined under fluorescence microscopy. ImageJ software was utilized for quantitative analysis of the fluorescence intensity.

#### Therapeutic efficacy of HA-NG/TAC in vivo

Following the second immunization, CIA mice were established and evaluated every other day in accordance with the aforementioned protocol. We assessed every mouse individually using a scale of 0 to 4. 0, no evidence of erythema and swelling; 1, erythema and mild swelling confined to the tarsals or ankle joint; 2, erythema and mild swelling extending from the ankle to the tarsals; 3, erythema and moderate swelling extending from the ankle to metatarsal joints; 4, erythema and severe swelling encompass the ankle, foot and digits, or ankylosis of the limb. Every mouse was given a total arthritis score based on its four paws. Once the model was established, the mice were divided into four groups at random and given PBS, TAC, NG/TAC, and HA-NG/TAC for treatment according to their clinical scores. Healthy DBA mice were treated as a control group. In CIA mice, intravenous injections were given every two days after the 30th day of primary immunization. Following a period of 48 days after the primary immunization, the mice were sacrificed.

#### Histological and immunofluorescent assay

Following the sacrifice of the arthritis mice, the organs (heart, liver, spleen, lung, kidney) and hind knee joints were collected and combined in a solution of 4% paraformaldehyde. Subsequently, the joints were decalcified for a period of 30 days using a 20% (w/v) ethylenediaminetetraacetic acid (EDTA) solution, and then sliced. Subsequently, the tissue slides underwent staining with H&E. Two researchers evaluated the Histological Synovitis Scores (HSS) (Supplementary Table 3), and the outcomes were determined based on the mean scores. The tissue sample slides were blocked with 5% BSA and treated with antibodies targeting IL-1$\beta$, IL-6, and TNF-$\alpha$. To identify these pro-inflammatory cytokines in the tissue slides, a fluorescence microscope was utilized.

#### Micro-CT reconstruction and analysis

We used Mimics software to generate 3D images of the hind paw joints by scanning them with a Micro-CT scanner at a resolution of 15 μm. A quantitative analysis of bone mineral density (BMD), the rate of bone volume and total volume (BV/TV), trabecula number (Tb. N), trabecula spacing (Tb. Sp), and trabecula thickness (Tb. Th) was performed using CTAn software.

#### Expression level of pro-inflammatory cytokines in vivo

ELISA kits were used to detect the serum levels of IL-1$\beta$, IL-6, and TNF-$\alpha$ in each group, following the manufacturer's instructions. To evaluate the samples, a microplate reader was utilized with wavelengths of 450 nm and 630 nm. After crushing the hind knee joints of CIA mice in liquid nitrogen and extracting the supernatant, we obtained total RNA using TRIZOL. Afterwards, the trichloromethane and isopropanol were used to purify the total RNA. Strand cDNA Synthesis Super Mix kit instructions were followed to synthesize cDNA. IL-1$\beta$, IL-6, and TNF-$\alpha$ mRNA were successfully detected through

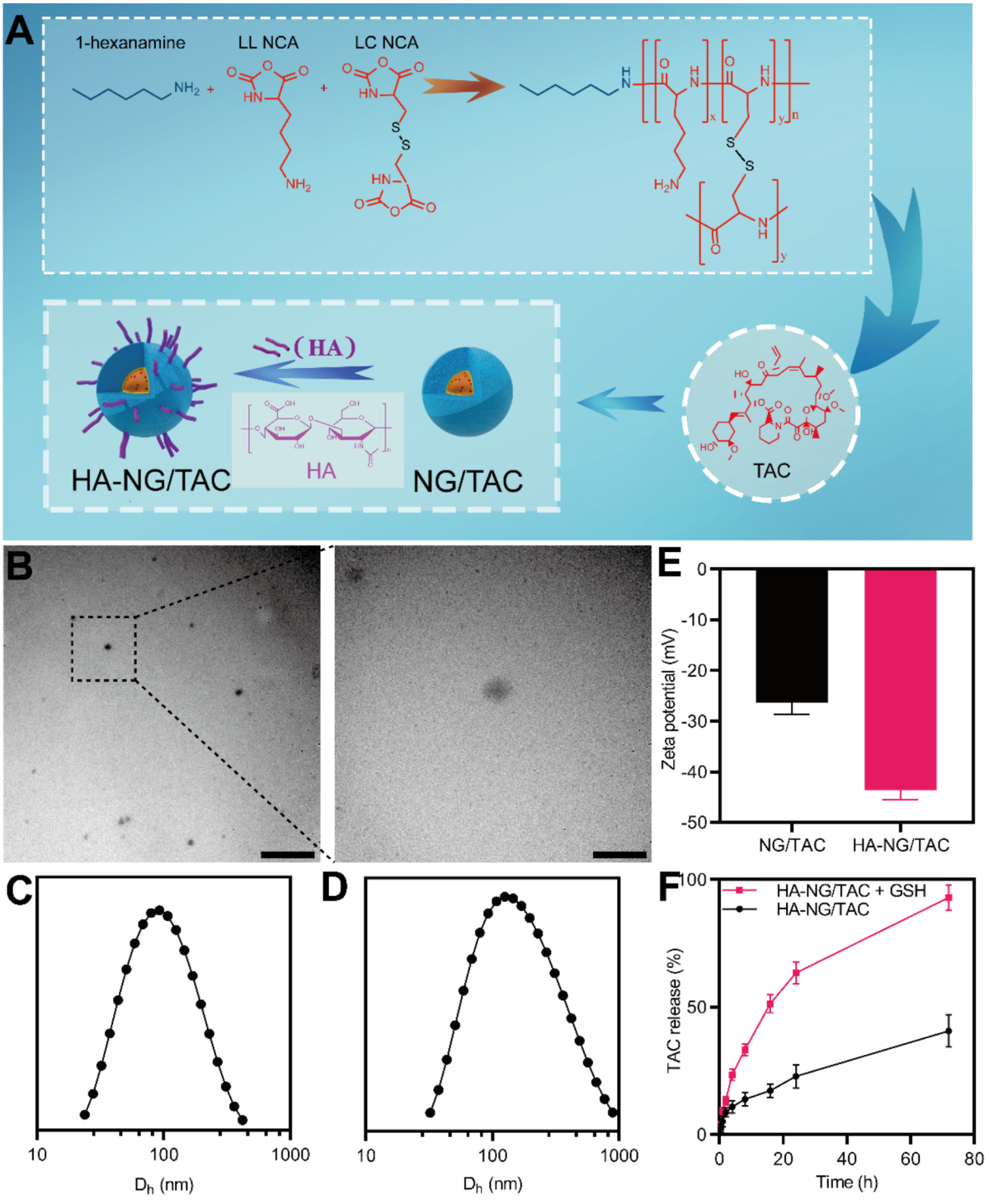


**Fig. 1** HA-NG/TAC was prepared and characterized. (**A**) An outline is provided to illustrate the process of preparing HA-NG/TAC. (**B**) TEM images representing HA-NG/TAC ($n=3$). Scale bar = 1 μm (low power); 0.2 μm (high power). C-D The illustration of DLS datum distribution of (**C**) NG/TAC and (**D**) HA-NG/TAC. (E) Zeta potential of NG/TAC and HA-NG/TAC ($n=3$). (**F**) The release of TAC from HA-NG with either 0 or 10 mM GSH in PBS at pH 7.4 was examined in vitro ($n=3$). The information is displayed as mean value ± SEM

a qPCR experiment utilizing qPCR SYBR Green Master Mix and an Agilent MX3000P instrument. GAPDH was used as a reference for standardized mRNA expression.

### Statistical analysis

Each experiment required a minimum of three trials. GraphPad Prism 9 was used to calculate the mean

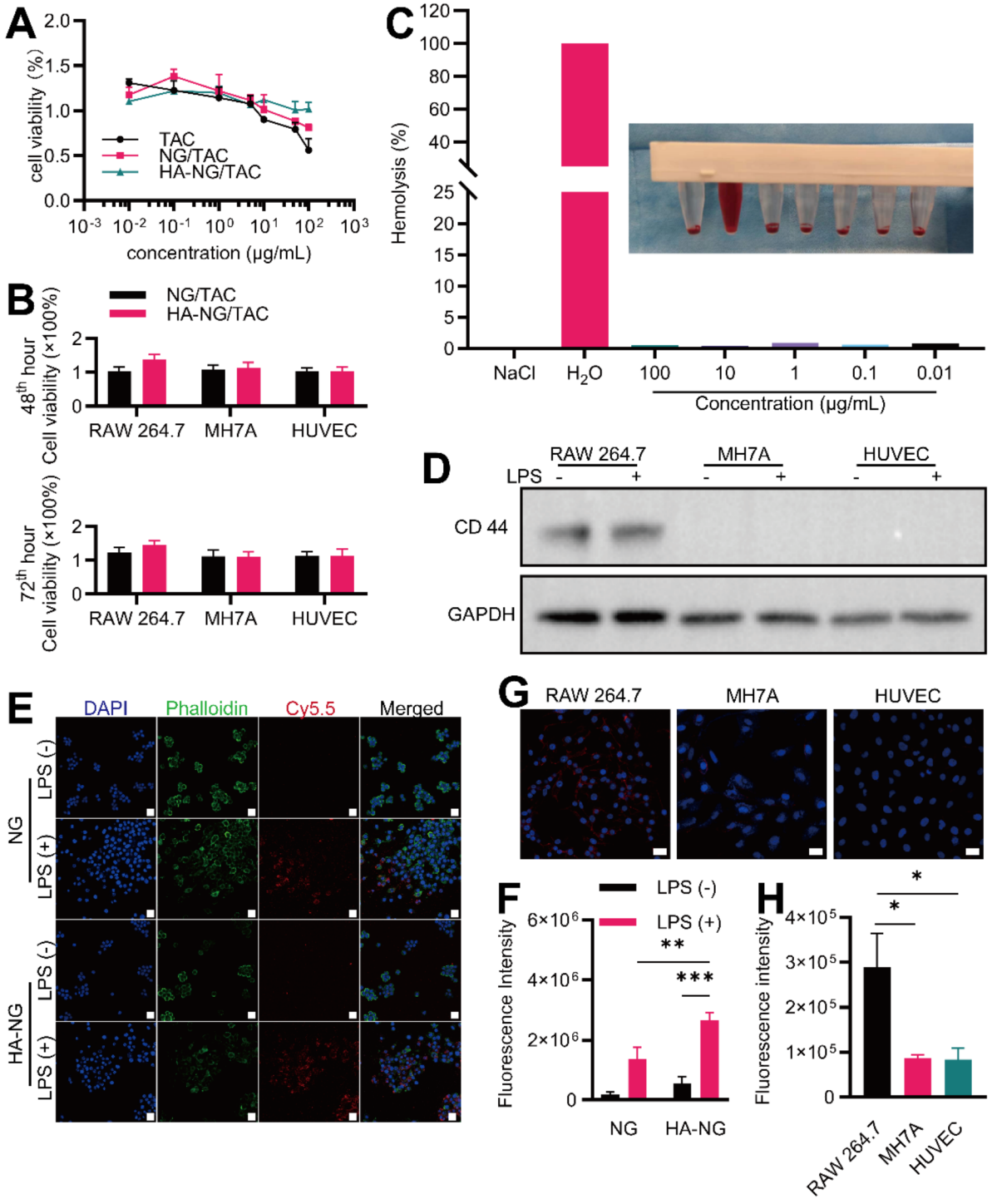


**Fig. 2** (See legend on next page.)

value±standard error of mean (SEM) based on the given number of experiments. An unpaired Student's t-test was used to compare two groups, while a one-way analysis of variance was used to analyze more than two groups. Significant differences were considered when p-value was less than 0.05.

(See figure on previous page.)

**Fig. 2** Effectiveness of HA-NG/TAC in vitro. (**A**) An analysis of HA-NG/TAC toxicity on normal macrophages was performed using the CCK-8 assay, followed by a comparison of these results with those for TAC and NG/TAC ($n=6$). The information is displayed as mean value ± SEM. (**B**) An analysis of toxicity on RAW 264.7, MH7A, and HUVEC treated with HA-NG/TAC for 48 h and 72 h was performed using the CCK-8 assay ($n=6$). The information is displayed as mean value ± SEM. (**C**) Hemolysis test of HA-NG/TAC. (**D**) Representative western blot image depicts the expression of proteins CD44 on RAW 264.7, MH7A, and HUVEC. (**E**) Fluorescent images depicting the engulfment of NG labelled with Cy5.5 and HA-NG labelled with Cy5.5 (in red) by RAW264.7 cells in both the LPS-treated and LPS-untreated groups ($n=3$). The nucleus is stained with DAPI (in blue) and the cytoskeleton structure is stained with SF488-Phalloidin (in green). The scale bar represents 50 μm. (**F**) Quantitative assessment of the fluorescence intensity in each group ($n=3$) was conducted using an unpaired student's t-test for statistical analysis. The results are presented as mean value ± SEM. Statistical significance was denoted as $^{*}p<0.05$, $^{**}p<0.01$, $^{***}p<0.001$, and $^{****}p<0.0001$. (**G**) Fluorescent images depicting the engulfment of NG labelled with Cy5.5 and HA-NG labelled with Cy5.5 (in red) by RAW 264.7, MH7A, and HUVEC treated by LPS ($n=3$). The nucleus is stained with DAPI (in blue). The scale bar represents 50 μm. (**H**) Quantitative assessment of the fluorescence intensity in each group ($n=3$) was conducted using ANOVA for statistical analysis. The results are presented as mean value ± SEM. Statistical significance was denoted as $^{*}p<0.05$, $^{**}p<0.01$, $^{***}p<0.001$, and $^{****}p<0.0001$

## Result

### Preparation and characterization of HA-NP/TAC

We synthesized 1-hexanamine-poly(L-lysine-co-L-cystine) using a ring-opening polymerization (ROP) method. L-lysine NCA and L-cystine NCA were reacted with the initiator 1-hexanamine, as shown in Fig. 1A. TAC was incorporated into the disulfide-core-cross-linked nanogel, with a drug loading content (DLC) of approximately 2.5 wt%. After mixing and stirring NG/TAC with HA for 24 h, the carboxyl terminus of HA and the amino terminus of NG/TAC underwent a dehydration condensation reaction. Figure 1B shows that HA-NG/TAC appeared as clear spherical structures under TEM. We then measured the average diameters of NG/TAC and HA-NG/TAC. Figure 1C and D show that NG/TAC had an average diameter of 77.4 nm, while HA-NG/TAC had an average diameter of 119 nm. These sizes are suitable for passive retention in inflamed joints via the EPR effect. HA-NG/TAC exhibited a lower surface zeta potential compared to NG/TAC (Fig. 1E), which enhanced its colloidal stability. The reduction-responsive HA-NG/TAC, containing disulfide bonds, could degrade in response to GSH in macrophages. As shown in Fig. 1F, less than 50% of TAC was released from HA-NG at 72 h under normal conditions. However, elevated GSH levels accelerated TAC release, resulting in over 90% TAC release, mimicking cellular conditions. HA-NG/TAC's active targeting capability not only minimized drug loss in the bloodstream but also promoted preferential accumulation in inflammatory macrophages.

### Effectiveness of HA-NG/TAC in vitro

TAC, an immunosuppressant used to treat autoimmune diseases like RA, shows beneficial anti-inflammatory properties. However, high doses of free TAC can have limited long-term effectiveness due to off-target effects. We evaluated HA-NG/TAC toxicity using cell viability assays on RAW 264.7 cells. Figure 2A shows that nanogel encapsulation significantly reduced TAC toxicity to normal macrophages. The nanogel degraded slowly due to low GSH levels and slow internalization rates. HA-NG also provided better protection for normal macrophages from high-dose TAC compared to NG/TAC (Fig. 2A). We assessed the cytotoxicity of NG and HA-NG on fibroblast-like synoviocytes (FLSs) and vein endothelial cells (Fig. 2B). Hemolysis assays demonstrated that HA-NG/TAC had low hemolysis rates, below 5%, across a concentration range of 0.01–100 μg/mL (Fig. 2C), indicating good biocompatibility and suitability for in vivo applications.

Macrophages release pro-inflammatory cytokines like IL-1β, IL-6, and TNF-α, which are crucial in RA pathology. Targeting activated macrophages in inflamed joints helps reduce the pro-inflammatory cytokine network. We validated by Western blot that only macrophages highly expressed CD44 in RAW264.7, MH7A, and HUVEC cells (Fig. 2D). Using CLSM, we examined the cellular absorption of Cy5.5-labeled HA-NG. Figure 2E shows significant fluorescence intensity in activated macrophages, while normal macrophages displayed low intensity. This suggests that HA-NG degrades within activated macrophages, which have high levels of reducing agents like GSH. Fluorescence quantitative analysis (Fig. 2F) showed higher intensity in activated macrophages treated with Cy5.5-labeled HA-NG compared to those treated with Cy5.5-labeled NG. The attachment of HA-NP to the cell surface intensified internalization in activated macrophages. We also evaluated HA-NG phagocytosis by FLS and HUVEC cells. Figure 2G shows that HA-NG was extensively phagocytosed by LPS-activated macrophages, while MH7A and HUVEC cells exhibited low phagocytosis rates. The differences were statistically significant (Fig. 2H). These results confirm that HA-NG/TAC specifically targets activated macrophages in the synovial microenvironment.

### Specific distribution of HA-NG/TAC in vivo

We analyzed the biodistribution and targeting of HA-NG/TAC in vivo using the CIA mouse model. Cy5.5-labeled nanogels were administered intravenously to arthritic mice when their clinical scores averaged 14. Figure 3A shows strong fluorescence in all joints of the HA-NG group, whereas the Cy5.5 group and the NG group had minimal fluorescence after 24 h. The EPR

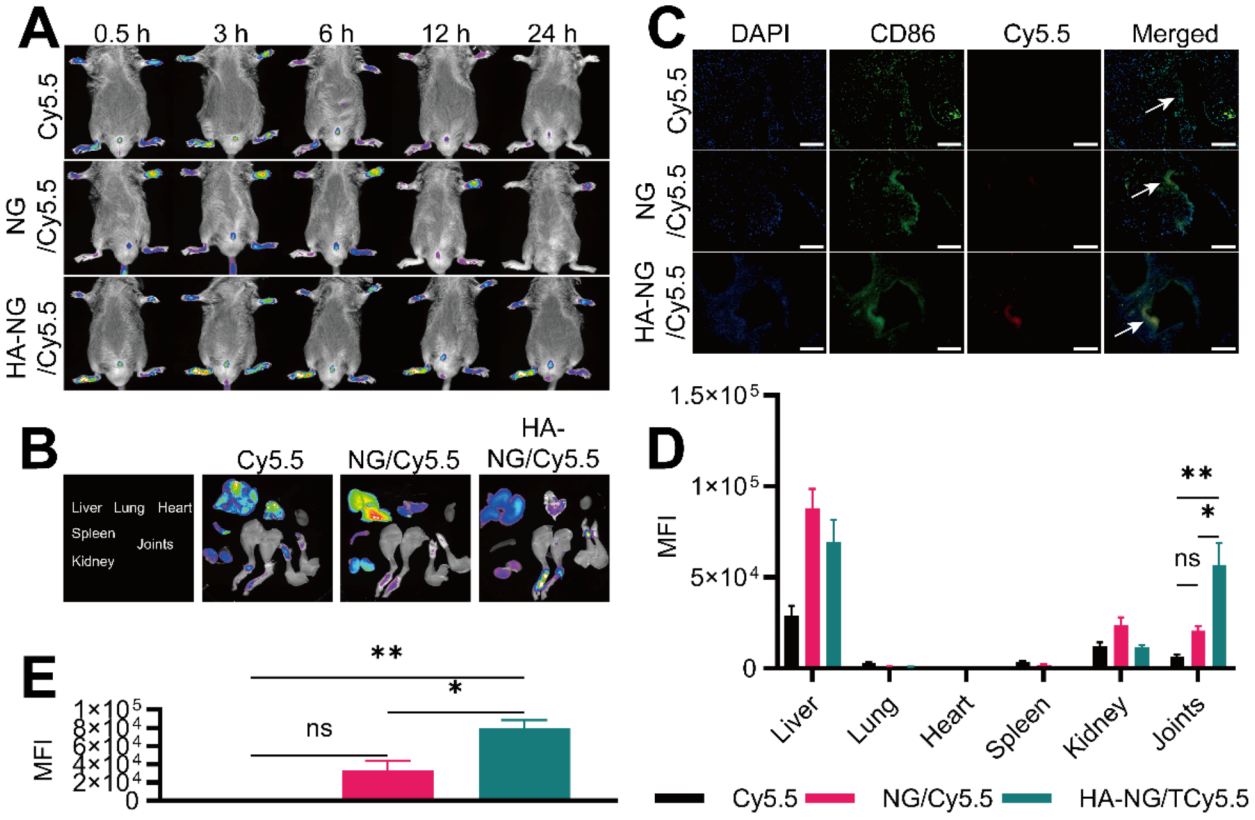


**Fig. 3** Distribution of HA-NG/TAC in CIA mice. (**A**) In vivo distribution of free-Cy5.5, Cy5.5-labeled NG and Cy5.5-labeled HA-NG in mice with collagen-induced arthritis (CIA) at the joints at the 0.5th, 3th, 6th, 12th, 24th hour post-injection. (**B**) The distribution of free-Cy5.5, NG labeled with Cy5.5 and HA-NG labeled with Cy5.5 in liver, lung, heart, spleen, and kidney at the 24th hour post-injection is shown. (**C**) The synovium's distribution of free-Cy5.5, NG labeled with Cy5.5, and HA-NG labeled with Cy5.5 can be observed in the representative fluorescence images. The nucleus is stained with DAPI (blue), macrophages were stained with AF488-CD86 (green), while free-Cy5.5, NG, or HA-NG are labeled with Cy5.5 (red). The measurement scale is 50 μm; white arrow: synovium. (**D**) The fluorescence intensity in various organs and joints was quantitatively analyzed ($n = 3$). The data are analyzed using ANOVA and presented as mean value ± SEM. (**E**) Quantitative evaluation of the fluorescence intensity of Cy5.5, NG labeled with Cy5.5 or HA-NG labeled with Cy5.5 within the activated macrophages of synovium was conducted ($n = 3$). The data were analyzed using ANOVA and are presented as mean ± SEM. Significance levels were indicated as $^{*}p < 0.05$, $^{**}p < 0.01$, $^{***}p < 0.001$, and $^{****}p < 0.0001$

effect allows Cy5.5-labeled NG to reach inflamed joints but also distributes it to other organs like the liver and kidney, leading to rapid elimination. In contrast, HA-coated NG effectively targets inflamed joints by binding to CD44, which is overexpressed on activated macrophages. Significant fluorescence was observed in the liver and kidney of the Cy5.5-labeled NG group, while Cy5.5-labeled HA-NG was primarily found in the liver. The smaller diameter of NG/TAC compared to HA-NG/TAC resulted in more filtration through the kidney, leading to greater HA-NG/TAC accumulation in inflamed joints. Quantitative fluorescence analysis revealed that the fluorescence intensity in inflamed joints of the Cy5.5-labeled HA-NG group was approximately three times higher than in the Cy5.5-labeled NG group, with significant statistical significance. Tissue sectioning and immunofluorescence staining with the activated macrophage marker CD86 showed that HA-NG accumulated more effectively in synovial tissue macrophages compared to NG. Quantitative fluorescence analysis confirmed superior accumulation of HA-NG. Thus, HA-coated reduction-responsive nanogels increased TAC concentration in inflamed joints of mice, particularly in activated macrophages, enhancing TAC treatment effectiveness while minimizing toxicity to other organs.

### Therapeutic efficiency of HA-NG/TAC in collagen-induced arthritis mice

To evaluate HA-NG/TAC's immunosuppressive efficiency in vivo, we used the CIA mouse model. Figure 4A shows that control mice received PBS, while arthritic mice received TAC, NG/TAC, and HA-NG/TAC intravenously on the 30th day following primary immunization. Paw swelling was initially used to measure arthritis progression. Mice treated with each formulation showed significant inflammation reduction by the 48th day

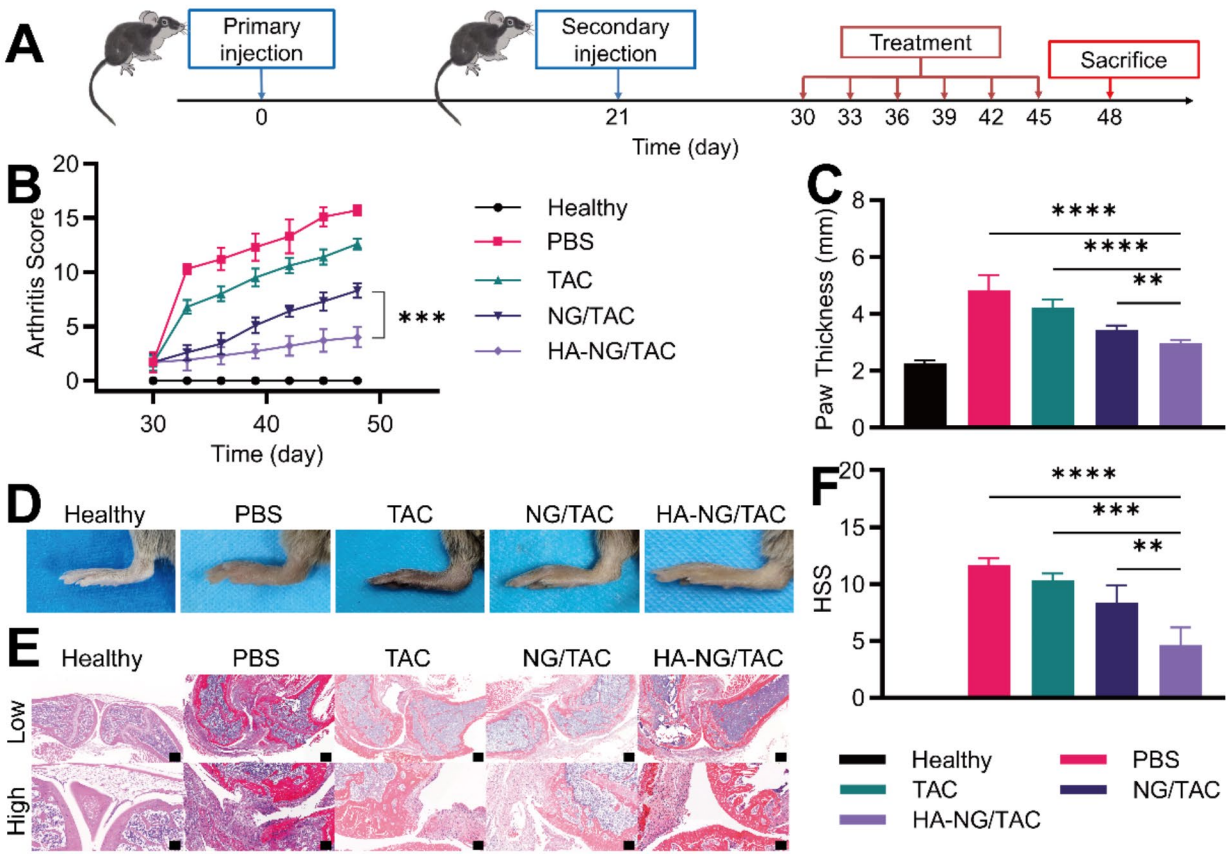


**Fig. 4** Therapeutic efficacy of HA-NG/TAC in CIA mice. (**A**) Progression of CIA mouse experiment timeline. **B-C** The impact of Healthy, PBS, TAC, NG/TAC, and HA-NG/TAC on arthritis score (**B**) and paw thickness (**C**) after the final treatment ($n = 10$) was assessed. Data analysis was conducted using ANOVA, and the results are presented as mean value ± SEM. Statistical significance was denoted as $^{*}p < 0.05$, $^{**}p < 0.01$, $^{***}p < 0.001$, $^{****}p < 0.0001$. (**D**) After the final administration of Healthy, PBS, TAC, NG/TAC, and HA-NG/TAC, photographs depicting the swollen joints of CIA mice were captured. (**E**) Illustrative H&E stain images of the synovial tissue in every group ($n = 3$); scale bar = 200 μm (low magnification), 50 μm (high magnification). (**F**) Synovitis histology test ($n = 3$); The data is analyzed using ANOVA, and the mean value ± SEM is shown; $^{*}p < 0.05$, $^{**}p < 0.01$, $^{***}p < 0.001$, $^{****}p < 0.0001$

compared to controls. The control group showed noticeable erythema and inflammation in the inflamed joints. The TAC and NG/TAC groups had comparable therapeutic effects, but HA-NG/TAC provided notable inflammation inhibition. Arthritis scores were assessed during treatment based on swelling and erythema. Prior to treatment, all groups had similar arthritis scores of approximately 1.7. The control group reached a peak arthritis score of 15.7. The arthritis scores for TAC, NG/TAC, and HA-NG/TAC were 12.6, 8.3, and 4, respectively. Paw thickness measurements on the 48th day matched these findings. The control group showed significant swelling, with an average paw thickness of approximately 4.84 mm. The average thicknesses for TAC, NG/TAC, and HA-NG/TAC were 4.22 mm, 3.44 mm, and 2.99 mm, respectively. Free TAC had minimal effect compared to controls, while NG/TAC and HA-NG/TAC showed significant reductions in arthritis scores and paw thickness.

Since paw swelling is an external indicator of RA, we conducted histopathological examinations for further analysis. Inflamed knee joints underwent H&E staining. We evaluated the Histological Synovitis Score (HSS) considering synovial inflammation and cartilage damage. The control group had the highest scores due to noticeable synovial growth, pannus formation, and extensive cartilage damage. The TAC group showed no significant differences from the control group. NG/TAC reduced synovial proliferation and protected cartilage from degradation. Mice treated with HA-NG/TAC showed the most effective therapy, with cartilage resembling healthy joints and minimal synovial cell layers. The HA-NG/TAC group had the lowest HSS, with statistical significance. Bone erosion, a prominent feature in late-stage RA, was assessed by Micro-CT analysis. Quantitative analysis of BMD, BV/TV, Tb. N, Tb. Th, and Tb. Sp showed significant differences. Figure 5A shows extensive bone erosion in the control group. TAC and NG/TAC did not

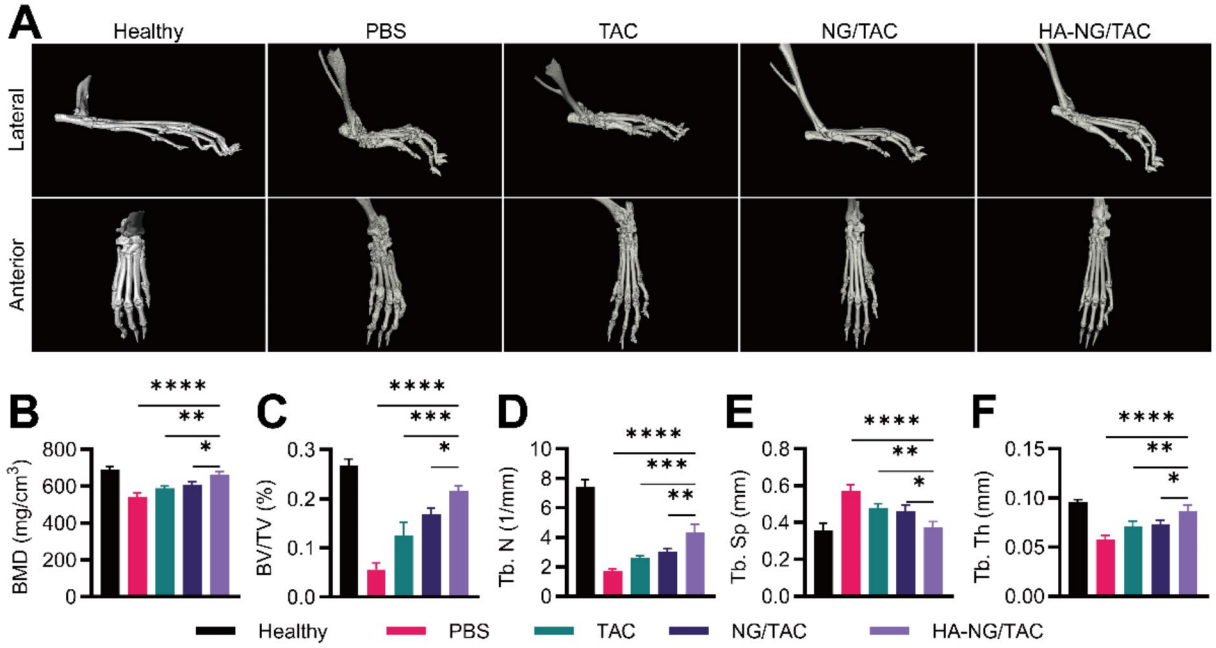


**Fig. 5** HA-NG/TAC prevented bone from erosion. (**A**) Representative reconstruction images of hind limbs of each group ($n = 3$). (**B**-**F**) Quantitative analysis of bone mineral density (BMD) (**B**), bone volume fraction (BV/TV) (**C**), trabecula number (Tb. N) (**D**), trabecula spacing (Tb. Sp) (**E**), trabecula thickness (Tb. Th) (**F**) ($n = 3$). The data were analyzed using ANOVA, and the results are presented as mean value ± SEM. Statistical significance was indicated as $^{*}p < 0.05$, $^{**}p < 0.01$, $^{***}p < 0.001$, and $^{****}p < 0.0001$

effectively prevent bone erosion, while HA-NG/TAC treatment significantly reduced it.

Additionally, we examined pro-inflammatory cytokine levels in mice with experimental arthritis. Immunofluorescent staining revealed TNF-α, IL-1β, and IL-6 in the synovium of inflamed knee joints across all groups (Fig. 6A). The control group showed widespread distribution of these cytokines, while the TAC group had slightly reduced levels. NG/TAC significantly decreased synovial cell proliferation and pro-inflammatory cytokine levels. The HA-NG/TAC group showed minimal fluorescence signals for these cytokines. ELISA results confirmed significant increases in cytokine expression in the control group. The other three groups showed varying degrees of suppression, with HA-NG/TAC having the lowest levels, indicating effective suppression of inflammation and reduced pro-inflammatory cytokine release into the serum (Fig. 6B-D). qPCR tests of mRNA expression for TNF-α, IL-1β, and IL-6 in hyperplastic synovium supported these results (Fig. 6E-G).

Finally, we assessed the chronic toxic effects of HA-NG/TAC. Figure 7 shows no apparent organic abnormalities following treatment with TAC, NG/TAC, and HA-NG/TAC. Thus, HA-coated reduction-responsive nanogels could be a promising option for future clinical use in RA patients.

## Discussion

The synovial microenvironment in RA shows chronic inflammation, increased oxidative stress, and a complex interaction of immune cells, cytokines, and other inflammatory mediators [9]. This pathological state triggers a series of cellular and molecular events that sustain the disease and lead to joint destruction [4]. High levels of ROS are a hallmark of RA, worsening tissue damage and maintaining the inflammatory response [10]. Initially, increased oxidative stress induces the upregulation of endogenous antioxidants like GSH to counteract ROS damage. However, as inflammation continues, GSH levels deplete, reducing the cell's capacity to effectively handle oxidative damage [13, 14]. This dynamic change in GSH is crucial as it drives inflammation and offers an opportunity for targeted therapeutic interventions. Activated immune cells, which have high levels of proliferation and differentiation, possess higher intracellular GSH levels compared to resting immune and stromal cells [16]. By exploiting the elevated GSH levels in activated macrophages, which are prevalent in inflamed tissues, novel drug delivery systems can be designed to release therapeutic agents specifically within the inflammatory microenvironment. This strategy enhances treatment efficacy and minimizes systemic side effects.

Our study used redox-responsive polyamino acid nanogels to deliver TAC specifically to inflamed joints. Disulfide bonds within the nanogel structure allow for controlled drug release in response to high GSH levels.

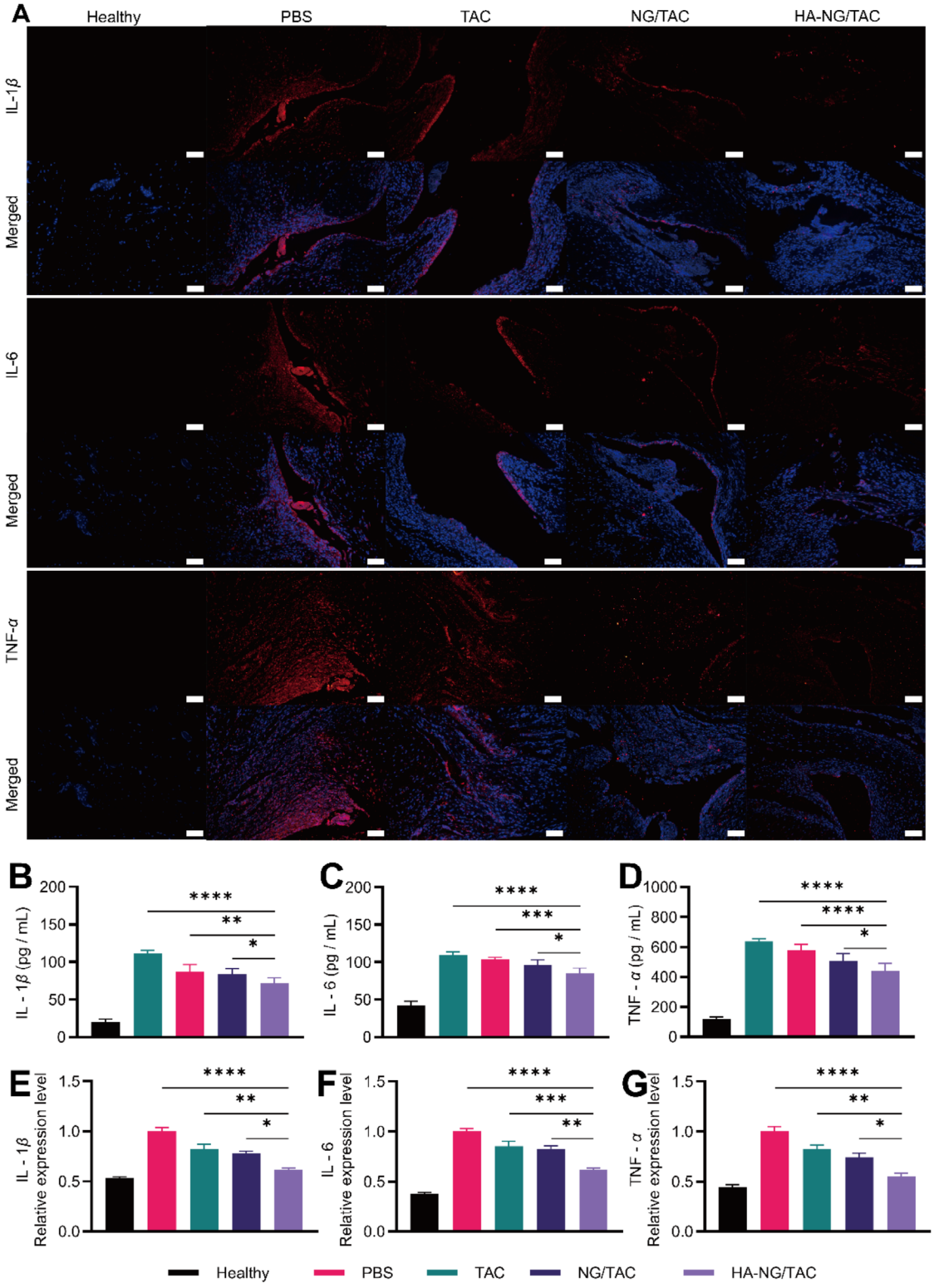


**Fig. 6** The effectiveness of HA-NG/TAC in reducing pro-inflammatory cytokines was observed in mice with CIA. (**A**) Immunofluorescent staining of the selected samples shows the existence of pro-inflammatory cytokines (red) such as TNF-*α*, IL-1*β*, and IL-6 ($n=3$). The nucleus is stained with DAPI (blue), and the scale bar measures 100 μm. B-D ELISA tests were used to determine the serum levels ofIL-1*β* (**B**), IL-6 (**C**),and TNF-*α* (**D**) in every group ($n=3$). **E-G** The qPCR method was used to determine the relative mRNA expression levels of IL-1*β* (**E**), IL-6 (**F**),and TNF-*α* (**G**) in the inflamed joints of each group, with a sample size of 3. The data is analyzed using ANOVA, and mean value ± SEM is displayed. The significance levels are denoted as $^{*}p<0.05$, $^{**}p<0.01$, $^{***}p<0.001$, and $^{****}p<0.0001$

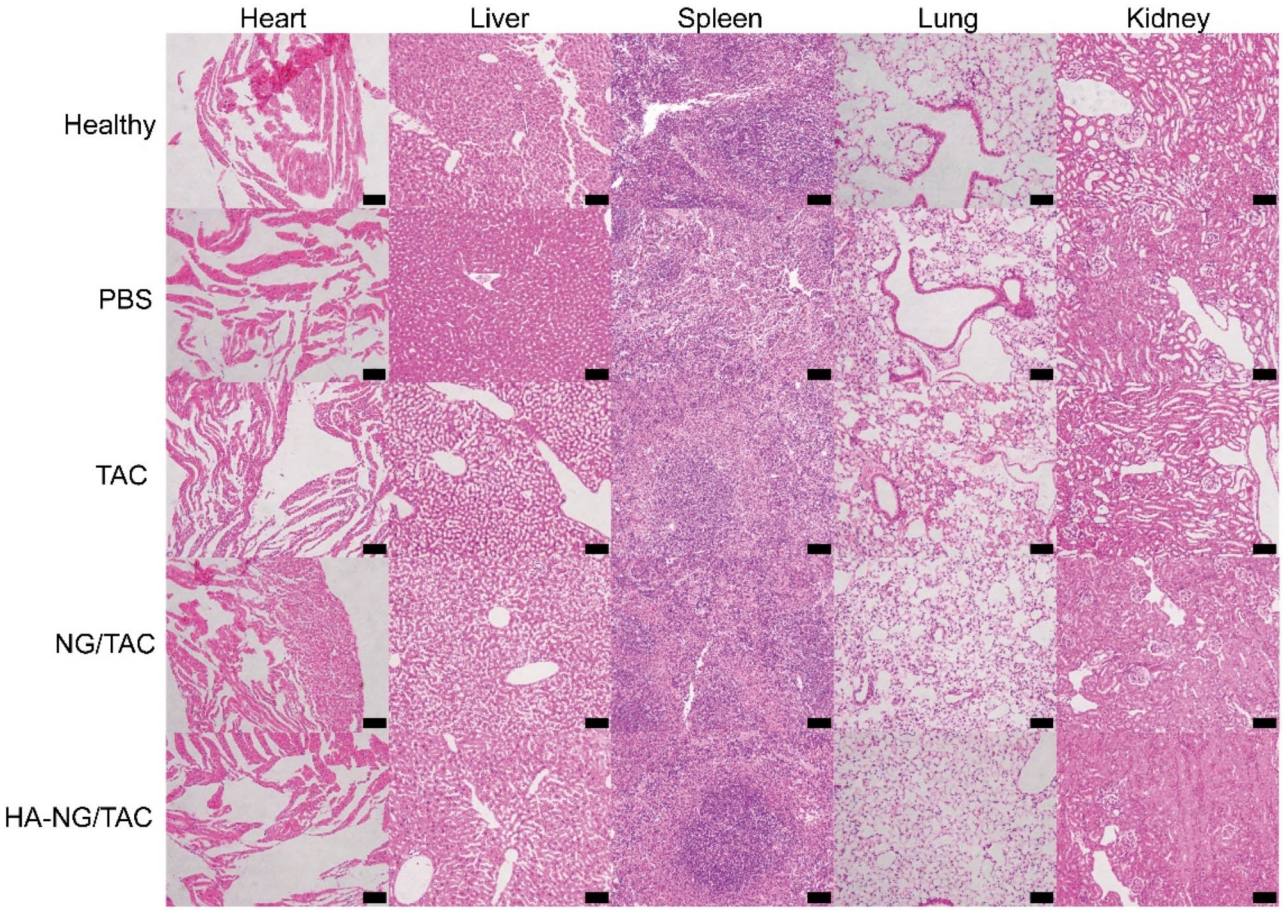


**Fig. 7** Chronic toxicity of HA-NG/TAC. H&E staining representative images of major organs in healthy mice or mice with experimental arthritis were observed. Scale bar = 100 μm

Under normal conditions, the nanogel remains stable, releasing less than 50% of TAC over 72 h. In the presence of elevated GSH levels, the disulfide bonds degrade, resulting in over 90% TAC release. This redox-responsive mechanism ensures that TAC is released specifically in the inflammatory environment, particularly within activated immune cells, rather than systemically. Controlled drug release improves the immunosuppressive efficacy of TAC by concentrating it in inflamed joints and reducing potential off-target effects and systemic toxicity.

To further enhance drug delivery specificity to activated macrophages in the inflamed synovium, we used HA. HA, a naturally occurring polysaccharide, binds to CD44 receptors overexpressed on activated macrophages and other inflammatory cells [26]. Conjugating HA with polyamino acid nanogels (HA-NG/TAC) significantly improved the targeting efficiency. In vivo experiments showed that HA-NG/TAC accumulated significantly more in inflamed joints compared to free-Cy5.5 and non-targeted NG/TAC. Fluorescence imaging demonstrated that HA-NG/TAC effectively localized to activated macrophages in the inflamed synovium, with minimal distribution to other organs, indicating successful active targeting. This HA-mediated targeting mechanism ensures precise delivery of therapeutic agents to inflammation sites, enhancing therapeutic efficacy and minimizing side effects.

Polyamino acid nanoparticles, composed of naturally occurring amino acids, exhibit excellent biocompatibility and biodegradability [28, 29]. They are safely metabolized and cleared from the body, minimizing the risk of adverse immune responses or long-term toxicity. Our study rigorously assessed the biocompatibility of HA-NG/TAC through various in vitro and in vivo experiments. The nanogels demonstrated low toxicity to normal macrophages and other cell types, including FLSs and endothelial cells, as indicated by cell viability assays and hemolysis tests. Low hemolysis rates confirmed that HA-NG/TAC is biocompatible and suitable for intravenous administration. Histopathological examinations and systemic toxicity assessments revealed no apparent organic abnormalities following HA-NG/TAC treatment, suggesting that the nanogels are well-tolerated and have a favorable safety profile.

## Conclusion

In conclusion, our research highlights the potential of HA-NG/TAC as a novel method for treating RA by addressing significant challenges in drug delivery and targeting. By exploiting the unique features of the synovial microenvironment, such as intracellular GSH levels, and using advanced targeting strategies with HA, we have developed a promising system to improve RA treatment outcomes. The demonstrated biocompatibility and efficacy in preclinical models suggest potential for future clinical applications, offering hope for more effective and safer therapies for individuals with RA and related inflammatory conditions.

## Supplementary Information

The online version contains supplementary material available at https://doi.org/10.1186/s12951-024-02784-y.

Supplementary Material 1

**Acknowledgements**

Thanks for the Key Laboratory of Polymer Ecomaterials, Changchun Institute of Applied Chemistry, Chinese Academy of Sciences, Changchun, PR China; Thanks for the Jilin Provincial Key Laboratory of Tooth Development and Bone Remodeling, Hospital of Stomatology, Jilin University, Changchun, P.R. China. Thanks for the Translational Medicine Experimental Platform of China-Japan Union Hospital of Jilin University.

**Author contributions**

Researchers MY and FC designed the experiments, and XW and YW characterized the properties of the biological drug carriers. YL, YG, and ZZ performed the animal experiments. Data analysis and interpretation were contributed by YL. ZZ, TL crafted all figures. The manuscript was edited and revised by MY, FC, XW, and YL.

**Funding**

The National Key Research and Development Program (Nos. 2022YFE0107700), the National Natural Science Foundation of China (Grant 32200611, 81701811), the Science and Technology Development Program of Jilin Province (Nos. 20210402006GH), the Science and Technology Development Program of Jilin Province (Grants 20240304072SF, 20190103087JH, 172410GG010135547, 222618JC010196569, 20220203120SF, 2023SC274, YDZJ202201ZYTS076, 2021SCZ40, 2018SCZ026, and 212558JC010486404), the Natural Science Foundation of Sichuan Province (Grant 2023NSFSC1600), and Funds for Bethune Program of Jilin University (Grant 2022B22) provided financial support for this research.

**Data availability**

No datasets were generated or analysed during the current study.

## Declarations

**Ethics approval and consent to participate**

The Institutional Animal Care and Use Committee of the Chinese Academy of Sciences gave its approval to all of the experiments.

**Consent for publication**

We have all given our consent for this manuscript to be published in the journal "*Journal of Nanobiotechnology*".

**Competing interests**

The authors declare no competing interests.

Received: 2 April 2024 / Accepted: 18 August 2024

Published online: 06 September 2024

**References**

1. Smith MH, Berman JR. What Is Rheumatoid Arthritis? Jama. 2022;327(12):1194.
2. Di Matteo A, Bathon JM, Emery P. Rheumatoid Arthritis Lancet. 2023;402(10416):2019–33.
3. Gravallese EM, Firestein GS. Rheumatoid arthritis - common origins, divergent mechanisms. N Engl J Med. 2023;388(6):529–42.
4. Komatsu N, Takayanagi H. Mechanisms of joint destruction in rheumatoid arthritis - immune cell-fibroblast-bone interactions. Nat Rev Rheumatol. 2022;18(7):415–29.
5. Smolen JS. Insights into the treatment of rheumatoid arthritis: a paradigm in medicine. J Autoimmun. 2020;110:102425.
6. Fereig SA, et al. Tacrolimus-loaded chitosan nanoparticles for enhanced skin deposition and management of plaque psoriasis. Carbohydr Polym. 2021;268:118238.
7. Kim JW, et al. Methotrexate, leflunomide and tacrolimus use and the progression of rheumatoid arthritis-associated interstitial lung disease. Rheumatology (Oxford). 2023;62(7):2377–85.
8. Zheng Z, et al. Effect of Tacrolimus vs Intravenous Cyclophosphamide on Complete or partial response in patients with Lupus Nephritis: a Randomized Clinical Trial. JAMA Netw Open. 2022;5(3):e224492.
9. Fearon U, et al. Cellular metabolic adaptations in rheumatoid arthritis and their therapeutic implications. Nat Rev Rheumatol. 2022;18(7):398–414.
10. Wu J, et al. TNF antagonist sensitizes synovial fibroblasts to ferroptotic cell death in collagen-induced arthritis mouse models. Nat Commun. 2022;13(1):676.
11. Yang Y, et al. Targeted silver nanoparticles for rheumatoid arthritis therapy via macrophage apoptosis and re-polarization. Biomaterials. 2021;264:120390.
12. Zhao W, et al. GGT5: a potential immunotherapy response inhibitor in gastric cancer by modulating GSH metabolism and sustaining memory CD8 + T cell infiltration. Cancer Immunol Immunother. 2024;73(7):131.
13. Wang N, et al. AMPK-a key factor in crosstalk between tumor cell energy metabolism and immune microenvironment? Cell Death Discov. 2024;10(1):237.
14. Rufino AT, et al. Rheumatoid arthritis molecular targets and their importance to flavonoid-based therapy. Med Res Rev. 2024;44(2):497–538.
15. Dang LH, et al. Thermally-responsive and reduced glutathione-sensitive folate-targeted nanocarrier based on alginate and pluronic F127 for on-demand release of methotrexate. Int J Biol Macromol. 2024;263(Pt 1):130227.
16. Zhang M, et al. Advanced application of stimuli-responsive drug delivery system for inflammatory arthritis treatment. Mater Today Bio. 2022;14:100223.
17. Ding H, et al. Preparation and application of pH-responsive drug delivery systems. J Control Release. 2022;348:206–38.
18. Li C, et al. Immunomodulatory nano-preparations for rheumatoid arthritis. Drug Deliv. 2023;30(1):9–19.
19. Feng N, Guo F. Nanoparticle-siRNA: a potential strategy for rheumatoid arthritis therapy? J Control Release. 2020;325:380–93.
20. Wang J, et al. X-ray-responsive polypeptide nanogel for concurrent chemoradiotherapy. J Control Release. 2021;332:1–9.
21. Li Z, et al. A tumor microenvironments-adapted Polypeptide Hydrogel/Nanogel Composite boosts Antitumor Molecularly targeted inhibition and immunoactivation. Adv Mater. 2022;34(21):e2200449.
22. Liu Y, et al. Olaparib and Doxorubicin Co-loaded Polypeptide Nanogel for enhanced breast Cancer therapy. Front Bioeng Biotechnol. 2022;10:904344.
23. Amruta A, et al. Vasculature organotropism in drug delivery. Adv Drug Deliv Rev. 2023;201:115054.
24. Srinivasarao M, Low PS. Ligand-Targeted Drug Delivery Chem Rev. 2017;117(19):12133–64.
25. Xu Z, et al. Hyaluronic acid-based glucose-responsive antioxidant hydrogel platform for enhanced diabetic wound repair. Acta Biomater. 2022;147:147–57.
26. Marinho A, Nunes C, Reis S. Hyaluronic acid: a key ingredient in the therapy of inflammation. Biomolecules, 2021. 11(10).
27. Brand DD, Latham KA, Rosloniec EF. Collagen-induced Arthritis Nat Protoc. 2007;2(5):1269–75.
28. Yang JZ, et al. Controlled synthesis and Biomedical Applications of Cystine-based Polypeptide nanomaterials. Acta Polym Sinica. 2021;52(8):960–77.

29. Ding L, et al. Intracellular reduction-responsive molecular targeted nanomedicine for Hepatocellular Carcinoma Therapy. Front Pharmacol. 2021;12:809125.

## Publisher's note